

Article

Exploration of Methodologies for Developing Antimicrobial Fused Filament Fabrication Parts

Sotirios Pemas¹ , Eleftheria Xanthopoulou² , Zoi Terzopoulou^{2,*} , Georgios Konstantopoulos³,
Dimitrios N. Bikiaris² , Christine Kottaridi³ , Dimitrios Tzouvaras¹ and Eleftheria Maria Pechlivani^{1,*} 

¹ Centre for Research and Technology Hellas, Information Technologies Institute, 6th km Charilaou-Thermi Road, 57001 Thessaloniki, Greece; sopemas@iti.gr (S.P.); dimitrios.tzouvaras@iti.gr (D.T.)

² Laboratory of Chemistry and Technology of Polymers and Colors, Department of Chemistry, Aristotle University of Thessaloniki, 54124 Thessaloniki, Greece; elefthxanthopoulou@gmail.com (E.X.); dbic@chem.auth.gr (D.N.B.)

³ Laboratory of General Microbiology, Department of Genetics, Development and Molecular Biology, School of Biology, Aristotle University of Thessaloniki, 54124 Thessaloniki, Greece; konstanto@bio.auth.gr (G.K.); ckottaridi@bio.auth.gr (C.K.)

* Correspondence: terzozoi@chem.auth.gr (Z.T.); riapechl@iti.gr (E.M.P.); Tel.: +30-2310-997818 (Z.T.); +30-2311-257751 (E.M.P.); Fax: +30-2310-474128 (E.M.P.)

Abstract: Composite 3D printing filaments integrating antimicrobial nanoparticles offer inherent microbial resistance, mitigating contamination and infections. Developing antimicrobial 3D-printed plastics is crucial for tailoring medical solutions, such as implants, and cutting costs when compared with metal options. Furthermore, hospital sustainability can be enhanced via on-demand 3D printing of medical tools. A PLA-based filament incorporating 5% TiO₂ nanoparticles and 2% Joncryl as a chain extender was formulated to offer antimicrobial properties. Comparative analysis encompassed PLA 2% Joncryl filament and a TiO₂ coating for 3D-printed specimens, evaluating mechanical and thermal properties, as well as wettability and antimicrobial characteristics. The antibacterial capability of the filaments was explored after 3D printing against Gram-positive *Staphylococcus aureus* (*S. aureus*, ATCC 25923), as well as Gram-negative *Escherichia coli* (*E. coli*, ATCC 25922), and the filaments with 5 wt.% embedded TiO₂ were found to reduce the viability of both bacteria. This research aims to provide the optimal approach for antimicrobial and medical 3D printing outcomes.

Keywords: additive manufacturing (AM); 3D printing; fused filament fabrication (FFF); filament; antimicrobial properties; *Escherichia coli*; *Staphylococcus aureus*; titanium dioxide (TiO₂); poly(lactic acid) (PLA); mechanical properties



Citation: Pemas, S.; Xanthopoulou, E.; Terzopoulou, Z.; Konstantopoulos, G.; Bikiaris, D.N.; Kottaridi, C.; Tzouvaras, D.; Pechlivani, E.M. Exploration of Methodologies for Developing Antimicrobial Fused Filament Fabrication Parts. *Materials* **2023**, *16*, 6937. <https://doi.org/10.3390/ma16216937>

Academic Editor: Roberto De Santis

Received: 9 October 2023

Revised: 19 October 2023

Accepted: 23 October 2023

Published: 29 October 2023



Copyright: © 2023 by the authors. Licensee MDPI, Basel, Switzerland. This article is an open access article distributed under the terms and conditions of the Creative Commons Attribution (CC BY) license (<https://creativecommons.org/licenses/by/4.0/>).

1. Introduction

Fused Filament Fabrication (FFF) technology is one of the most prevalent techniques in additive manufacturing (AM) [1–3] that has been developed exponentially [4,5]. This can be attributed to its rapid prototyping capabilities and cost-effective nature [6]. Due to the versatility that it provides, it can be applied for building every type of geometry from a variety of materials. The majority of the materials utilized in additive manufacturing applications consist of polymer-based composite materials and polymer blends [7] with the most commonly used in 3D printing of composite materials being Poly(lactic acid) (PLA) and acrylonitrile butadiene styrene (ABS) [8,9].

Poly(lactic acid) (PLA), a biobased and compostable polyester, finds diverse applications in tissue engineering, drug delivery, and medical applications [10–12]. It has been proven that when polymers are combined with specific nanoparticles, such as TiO₂, they acquire antimicrobial properties [13,14]. Titanium dioxide (TiO₂) has the ability to tune polymer properties such as antimicrobial activity, UV resistance, opacity, gas barrier, and color stability [7,15].

Numerous efforts have been documented in the literature with the aim of creating antimicrobial filaments for Fused Filament Fabrication (FFF) technology. Vidakis et al. [7] published a study that used (TiO₂) nanoparticles as nanofillers in order to enhance the properties of polypropylene (PP). The findings demonstrated that the characteristics (mechanical properties) of the nanocomposites had improved and it was demonstrated that PP/TiO₂ could be a nanocomposite system for use in AM applications. González et al. [16] examined PLA filled with TiO₂ nanoparticles in various particle content concentrations in a bacterial culture of *E. coli* and found that TiO₂ nanoparticles decreased the amount of extracellular polymeric substance and reduced bacterial growth. Also, no significant differences were observed for higher contents than 1% TiO₂ nanoparticles.

However, while most studies suggest that 3D-printed parts can be produced using antimicrobial filaments containing additives like TiO₂ with antimicrobial properties, this study examines a coating methodology to determine if it offers comparable results to the development of antimicrobial filaments. Implementing this coating technique in 3D-printed PLA components offers an alternative approach to imparting antimicrobial properties, bypassing the need to develop antimicrobial composite filaments for subsequent part fabrication through 3D printing. Although coating methodology has been used in scaffold applications to improve cell attachment/proliferation [17], here it is proposed as a method to provide antibacterial properties to medical 3D-printed parts and components or daily devices used in agri-food sector [6,18].

This study introduces an innovative approach to producing antimicrobial 3D-printed components through FFF AM technology. For the experiments, PLA was selected as the matrix material due to its biobased nature, as opposed to petroleum-based alternatives [19], and its favorable mechanical properties [20]. Given that FFF technology employs feedstock materials in filament form, the integration of TiO₂ nanoparticles into the filament is pursued to achieve antibacterial properties. The inclusion of Joncryl in small quantities as a chain extender enhances PLA's printability and mechanical properties by elevating molecular weight, complex viscosity, and melt flow index [21–23].

This work compares two methodologies for developing antibacterial 3D-printed components. The first method involves developing a composite filament that combines PLA, TiO₂, and Joncryl, suitable for use in all FFF 3D printers. A reference point is established by developing an additional filament made of PLA and Joncryl alone. The second method entails a coating process (dispersion immersion method) applied to the final parts manufactured using the PLA and Joncryl filament. These filaments were developed to produce specimens as a proof of concept for the future production of DIY (do-it-yourself) customized or pre-existing antimicrobial parts, medical tools, and more. All three specimen categories (1. PLA/Joncryl filament, 2. PLA/Joncryl/TiO₂ filament, and 3. PLA/Joncryl filament with a coating process) underwent comprehensive analysis, including physiochemical characterization and mechanical and antibacterial property assessments.

This paper is organized as follows: Section 2 outlines the materials and methods employed in the development of the present study. Section 3 encompasses the results, focusing on the characterization of the developed filaments and the coating methodology and presents data concerning their antibacterial activity and mechanical properties. Finally, the study concludes in Section 4. Figure 1 presents the architectural diagram of the methodology steps that were followed. These steps include the development of the filaments and the necessary tests conducted to extract results for characterizing the properties of the 3D-printed specimens.

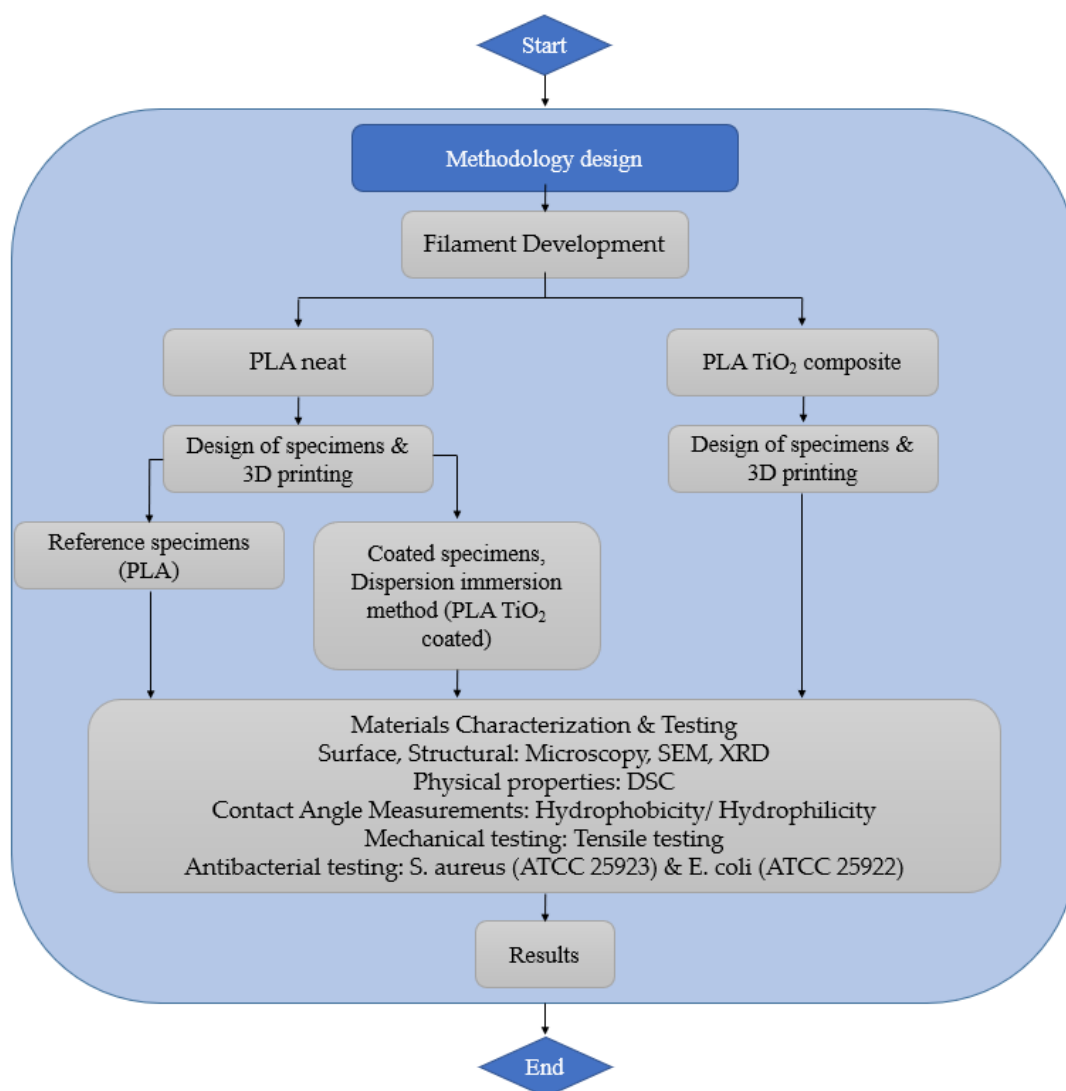


Figure 1. Architectural diagram.

2. Materials and Methods

2.1. Materials

In this study, the experimental materials used for the development of the filament included PLA in pellet form, Joncryl as a chain extender, and titanium dioxide (TiO₂) nanoparticles. The PLA pellets used were of PLA 4043D type, supplied by 3devo (Utrecht, The Netherlands). The chain extender Joncryl ADR[®] 4400 was supplied by BASF (Ludwigshafen, Germany). It possesses an epoxy equivalent weight of 485 g/mol and a weight-average molecular weight of 7100 g/mol. Aeroxide[®] TiO₂ P25 with a nanoparticle size of 21 nm and a specific surface area of 35–65 m²/g was supplied from Sigma-Aldrich (Saint Louis, MO, USA).

2.2. Development of a PLA-Based TiO₂ Filament

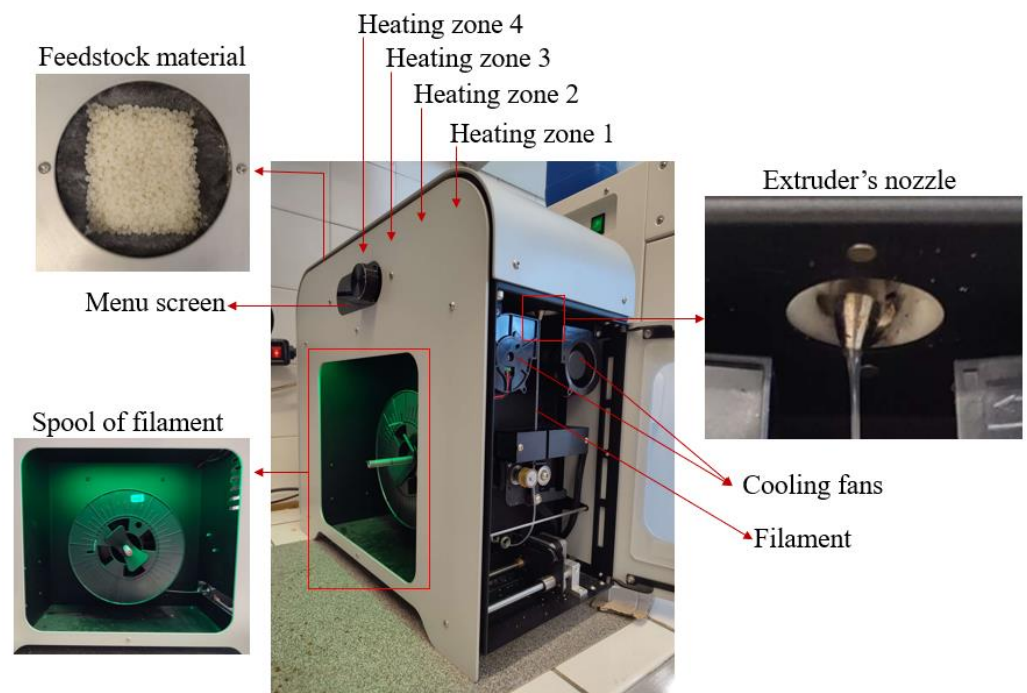
In order to develop the two distinct filaments based on PLA pellets, the PLA pellets were vacuum-dried overnight at 40 °C. The dried PLA was subsequently mixed with Joncryl to formulate the PLA/Joncryl filament (named as PLA), and with both Joncryl and TiO₂ to fabricate the potentially antimicrobial PLA/Joncryl/TiO₂ filament (named as PLA TiO₂ comp). Table 1 provides the composition of each filament. In total, 2 wt.% of Joncryl was used, and it was proven by Grigora et al. [24] in a previous work that it gives the best physicochemical properties to the final filament.

Table 1. Summary of Fabricated Filaments.

Composite Filaments	Experimental Materials		
	PLA (wt.%)	TiO ₂ (wt.%)	Joncryl (wt.%)
PLA/Joncryl	98%	-	2%
PLA/Joncryl/TiO ₂	93%	5%	2%

The filaments were fabricated using the 3devo Composer Series 350/450 filament maker (Utrecht, The Netherlands). Parameters were configured for extrusion of a 1.75 mm diameter filament. However, due to variations, the filament thickness deviation was ± 0.06 , resulting in a final filament diameter ranging between 1.69 mm and 1.81 mm. The machine contains a mixing screw that aids in material passage through four heating zones. Upon melting, the material is extruded as filament through a nozzle.

The four heating zones of the extruder can be independently set to distinct temperature values. In this experiment, temperature ranged from 175 °C to 192 °C. Various combinations were tested to optimize filament extrusion. Ultimately, the optimal temperature combination was found to be Heater 1—180 °C, Heater 2—192 °C, Heater 3—187 °C, and Heater 4—175 °C. Heater 1 is closest to the nozzle, while Heater 4 is situated near the hopper. The extruder's screw rotational speed, driving material through the heating zones and extruder, was set at 4.1 rpm. For filament cooling, integrated fans were adjusted to 60%, facilitating timely solidification for spool collection during fabrication. Figure 2 illustrates the characteristic components of the 3devo filament maker.

**Figure 2.** 3devo Filament Maker Overview.

2.3. Fabrication of 3D-Printed Specimens

After the successful development of both filaments, the FFF technology was used to fabricate the specimens. All specimens were designed using SOLIDWORKS® CAD Software (2022 SP2.0 Professional version) and manufactured utilizing an Original Prusa i3 MK3S+ 3D printer. Each part's 3D printing parameters were established using Prusa Slicer 2.5.0 software. For the PLA/Joncryl filament, the nozzle temperature was set at 220 °C, while for the PLA/Joncryl/TiO₂ filament, it was set at 240 °C. The bed temperature for

both filaments was set at 60 °C. In all cases, a 0.4 mm nozzle and 0.2 mm layer height were employed. The specimens from both filaments were printed with a 100% fill density and concentric fill pattern for infill. Settings not explicitly mentioned in the FFF process were maintained at their default values as per the Prusa Slicer software™ (Version 2.6.1) utilized in this study. Table 2 presents the specimens, along with their dimensions, used in the present study to characterize the properties of the 3D-printed specimens fabricated with the developed filaments.

Table 2. 3D-Printed Specimens.

Type of Test	Dimensions of 3D-Printed Specimens
Scanning Electron Microscopy (SEM)	10 × 2 × 1 mm
Tensile	ASTM D638 Standard, Type V [25]
Antibacterial	Φ 5 mm × 1 mm

The dimensions of the specimens were determined by the requirements of the testing equipment: Φ 5 mm × 1 mm for antibacterial testing and 10 × 2 × 1 mm for Scanning Electron Microscopy (SEM). Figure 3 displays the filament reels for the Prusa 3D printer, used to produce these specific specimens in two different surface configurations. Notably, the Φ 5 mm × 1 mm specimens provided satisfactory results, making the larger surface specimens redundant for antibacterial testing.

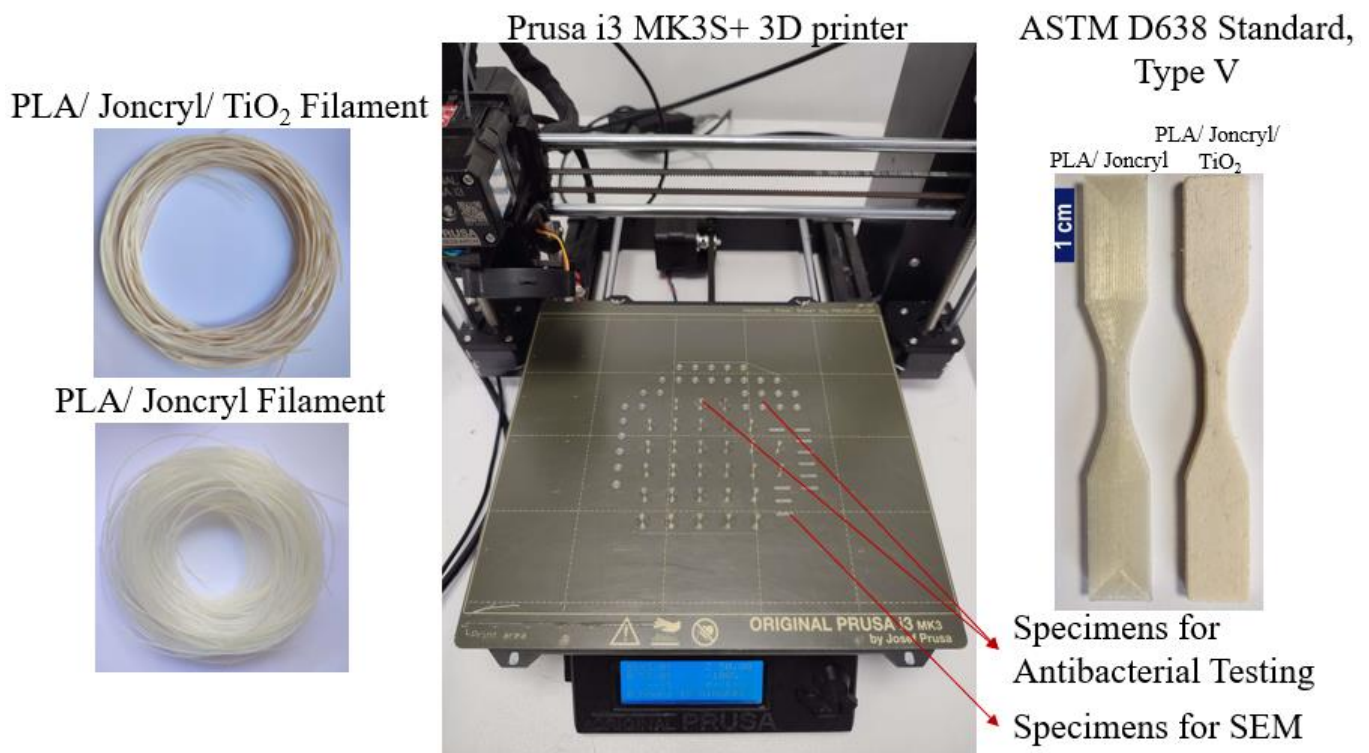


Figure 3. 3D Printer and Printed Specimens Visual Overview.

2.4. Coating Methodology: Dispersion Immersion Method

Between the two developed filaments, the PLA/Joncryl filament was selected for 3D printing the specimens that subsequently underwent a dispersion immersion coating process (as shown in Figure 4) to confer antimicrobial properties.

For the coating procedure, initially, the samples were immersed in a 1 M aqueous ammonia (NH₃) solution (pH = 11.5) and subjected to magnetic stirring at a speed of 435 rpm for 4 h at room temperature. Simultaneously, a 2 wt.% aqueous dispersion of TiO₂ was prepared. This dispersion underwent magnetic stirring for 1 h at a speed of

950 rpm, to prevent sedimentation in the stirring vessel. Around 30 min prior to removing the samples from the ammonia solution, an ultrasonication process was initiated using an ultrasonication probe. The process involved alternating cycles of 2 min of ultrasound treatment followed by 2 min of rest, repeated for a total of 6 cycles.

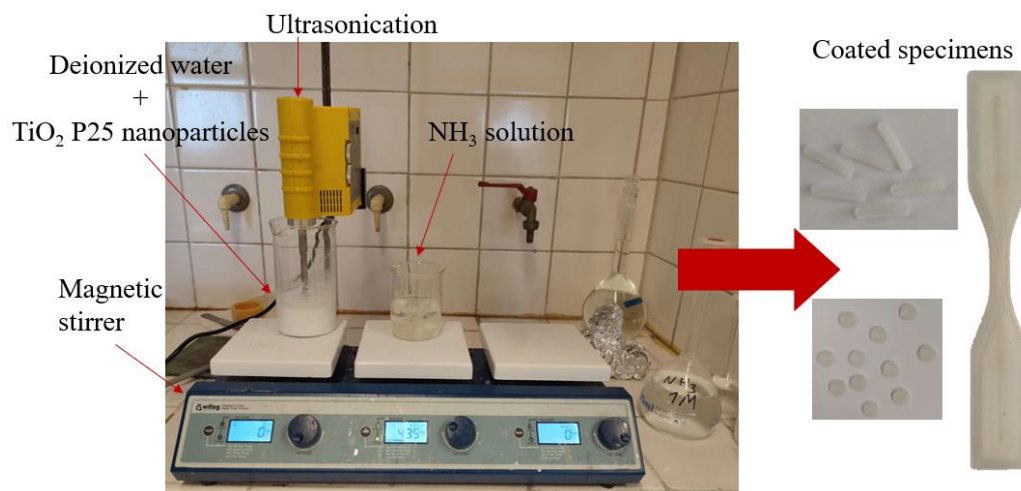


Figure 4. Coated specimens: materials and procedures used for dispersion immersion method.

After removal from the ammonia solution, the samples were thoroughly rinsed with deionized water and subsequently dried in an oven at 55 °C for 30 min. The dispersion containing deionized water and TiO₂ was heated at 70 °C and stirred magnetically for 30 min, with a stirring speed of 1200 rpm. Following this, the samples were immersed in this dispersion. The TiO₂ dispersion (with the specimens immersed) was heated to 70 °C and stirred magnetically at a speed of 875 rpm for a duration of 2 h. Afterwards, it was sonicated for 10 min, while maintaining the temperature at 70 °C. Finally, the samples were washed with ethanol and placed in an oven set at 75 °C for 10 min to facilitate drying. Upon completion of the aforementioned steps, the coating process concluded, resulting in the adhesion of TiO₂ powder particles to the samples (named as PLA TiO₂ coated).

2.5. Materials Characterization

2.5.1. Microscopy

The filaments' morphological features were examined with a stereoscope. Images were taken using a Jenoptik (Jena, Germany) ProgRes GRYPHAX Altair camera attached to a ZEISS (Oberkochen, Germany) SteREO Discovery V20 microscope and Gryphax image capturing software was used.

2.5.2. Scanning Electron Microscopy (SEM)

Scanning Electron Microscopy (SEM) images were captured using a JEOL (Tokyo, Japan) 2011 (JMS-840) electron microscope, equipped with an Oxford (Abingdon, UK) ISIS 300 energy-dispersive X-ray (EDX) micro-analytical system. Every specimen was positioned on the holder and coated with carbon to enhance the conductivity for the electron beam. The images were taken under an accelerating voltage of 2 kV, a probe current of 45 nA, and a counting time of 60 s.

2.5.3. X-ray Diffraction (XRD)

X-ray Diffraction (XRD) analyses of the polymers and copolymers were executed across a 2θ range of 5 to 80°, at intervals of 0.05°, and a scanning speed of 1.5 deg/min. The assessments were conducted using a MiniFlex II XRD system from Rigaku Co. (Tokyo, Japan) with Cu Kα radiation (λ = 0.154 nm).

2.5.4. Differential Scanning Calorimetry (DSC)

A PerkinElmer Pyris DSC-6 differential scanning calorimeter, which was calibrated with pure indium and zinc standards, was employed for the analysis. Samples of 5 ± 0.1 mg sealed in aluminum pans were used and all experiments were performed under N_2 atmosphere with a flow rate of 20 mL/min. Each specimen was subjected to a heating process from room temperature to 200 °C at a pace of 20 °C/min, then cooled down to 25 °C at the same rate of 20 °C/min and reheated to 200 °C at a 20 °C/min. The degree of crystallinity (X_c) was determined using Equation (1):

$$X_c(\%) = \left(\frac{\Delta H_m - \Delta H_{cc}}{\Delta H_f^0 - \frac{1 - \text{wt. \% additive}}{100}} \right) \times 100 \quad (1)$$

where ΔH_m , ΔH_{cc} , and ΔH_f^0 are the experimental melting enthalpy, the cold crystallization enthalpy, and the theoretical heat of fusion of 100% crystalline PLA ($\Delta H_f^0 = 93$ J/g), respectively.

2.5.5. Contact Angle Measurements

The water contact angle (WCA) was assessed with the Ossila (Sheffield, UK) Contact Angle Goniometer L2004A. The analysis of WCA for the samples was conducted through the sessile drop technique. A quantity of 25 μ L of distilled water was delicately placed atop the surface of the 3D-printed plates ($n = 3$) and scaffolds. High-resolution images were captured within a span of 20 s and further analyzed using the Ossila Contact Angle Software v3.1.1.0. The statistical evaluation was conducted through a one-way ANOVA followed by a post hoc Tukey test, facilitated by the GraphPad Prism 6 software. A p -value of less than 0.05 was deemed as indicative of statistical significance.

2.5.6. Tensile Testing

Tensile testing evaluations were conducted utilizing a Shimadzu EZ Test Tensile Tester, Model EZ-LX, equipped with a 2 kN load cell, following the ASTM D638 standards at a crosshead speed of 5 mm/min. For the testing, 3D-printed dumb-bell-shaped tensile type V test specimens were employed. Each sample underwent at least five separate assessments with the resulting data averaged to derive the mean values for Young's modulus, stress at break, and elongation at break. Data analysis was performed using one-way ANOVA, followed by a post hoc Tukey test, facilitated by GraphPad Prism 6 software. A p -value under 0.05 was established as the threshold for statistical significance.

2.5.7. Antibacterial Testing Methodology

Gram-positive *Staphylococcus aureus* (*S. aureus*, ATCC 25923), as well as Gram-negative *Escherichia coli* (*E. coli*, ATCC 25922) single colonies were inoculated in 10 mL of freshly prepared Nutrient Broth and incubated with agitation until reaching an OD600 measurement equal to 0.3–0.5. Then, 2 mL of the culture was moved to a microcentrifuge tube, spun for 1 min at 10,000 g, and the supernatant was removed. The cell pellet was resuspended in 2 mL PBS and spun for 1 min at 10,000 g. PBS washing was repeated twice. After the last spin, the pellet was resuspended in 2 mL PBS and 500 μ L was transferred in four different glass flasks containing 4.5 mL PBS. Serial dilutions of each flask were transferred on Nutrient Agar plates using a bent glass pipette and incubated overnight at 37 °C to determine the initial cfu/mL for each flask. After transferring to the plates, a control filament was added in one of the flasks, a TiO_2 -based filament was added to the second, a filament coated with TiO_2 was added to the third, whereas the last flask was used as a no filament control. The flasks were incubated for 1 h at 37 °C and 250 rpm, and then serial dilutions for each flask were transferred to fresh Nutrient Agar plates again. This procedure was repeated after one more hour of the flasks' incubation. The plates were left to incubate overnight at 37 °C. The number of colonies that represent the surviving bacteria

was counted the following day and the possibility of antibacterial activity of the filament was determined.

The filaments' antibacterial effectiveness against *S. aureus* and *E. coli* is reported as the mean standard deviation (SD) after 60 and 120 min of contact. Each experimental procedure was replicated three times ($n = 3$) for each bacterium strain. For statistical analysis, two-way ANOVA with repeated measurements was performed.

3. Results and Discussion

3.1. Scanning Electron Microscopy (SEM) and Optical Microscopy

The morphological characteristics and the dispersion of the TiO₂ nanocomposites in the polymer matrices are examined via microscopic techniques. Figure 5 displays the side surface of randomly selected 3D-printed tensile test specimens, providing a quantitative assessment of interlayer fusion, interlayer defects, or possible inhomogeneities.

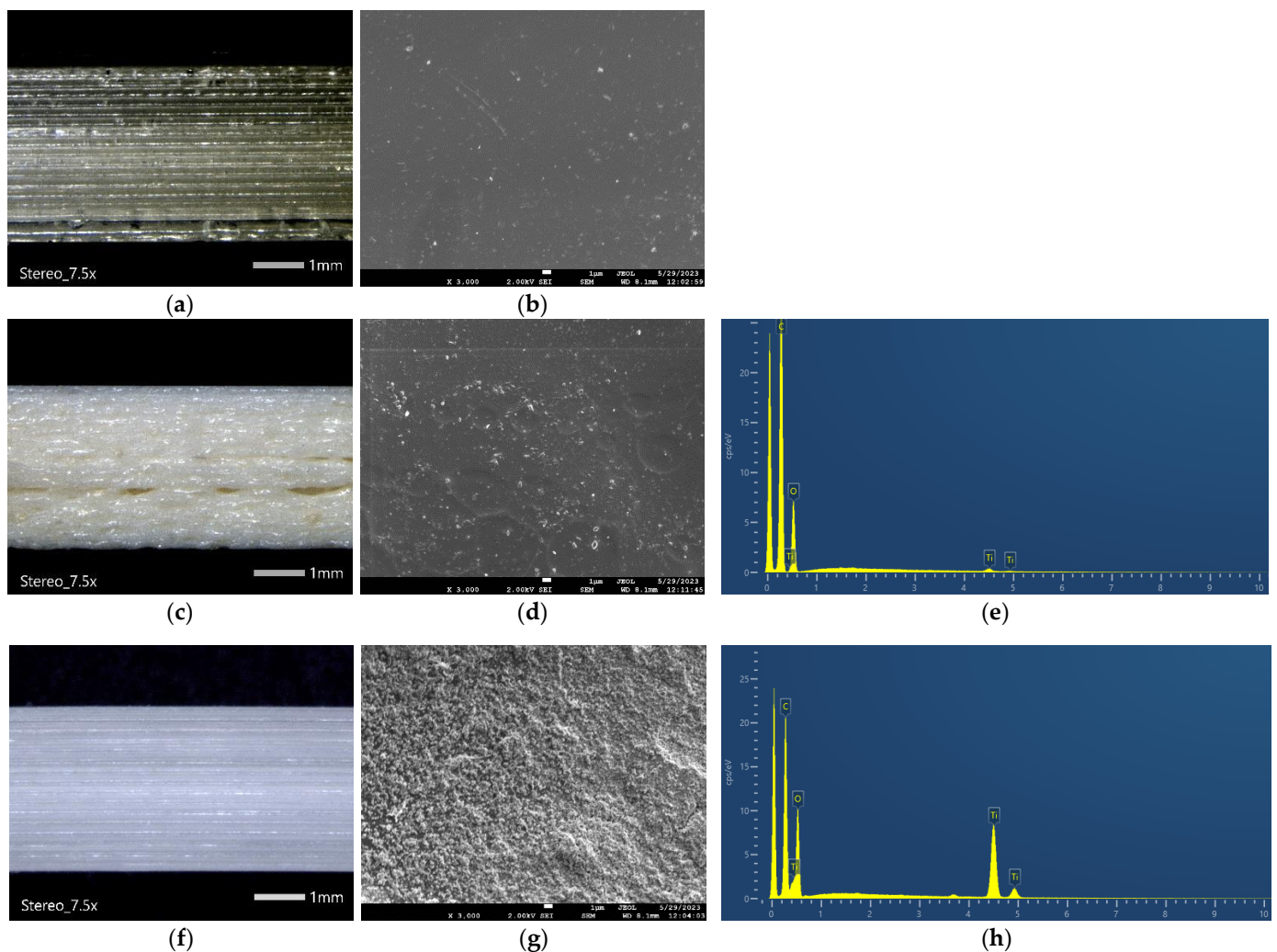


Figure 5. (a,b) Optical microscopy and SEM image of 3D-printed PLA (PLA/Joncryl filament), (c,d) optical microscopy and SEM image of 3D-printed PLA TiO₂ comp (PLA/Joncryl/TiO₂ filament), (e) EDX spectrum of 3D-printed PLA TiO₂ comp, (f,g) optical microscopy and SEM image of 3D-printed PLA TiO₂ coated, and (h) EDX spectrum of 3D-printed PLA TiO₂ coated.

It can be observed in Figure 5a,c,f that the 3D printing process utilizing the PLA/Joncryl/TiO₂ filament does not yield the same 3D printing quality as the PLA/Joncryl filament. This difference arises from the formation of TiO₂ nanoparticles' agglomerates, resulting in inconsistent material extrusion flow. This phenomenon is strongly associated with

the dimension and the weight fraction of the inorganic additive in the polymer matrix. Specifically, it was found that >1 wt.% of additive led to an increased agglomeration, and thus, intense surface roughness [26–28]. Furthermore, the processing method seems to affect the morphological features of the final specimen. Specifically, the dispersion of TiO_2 particles is observed to be more homogeneous in the case of the composite, resulting in a smooth surface. On the contrary, the coating procedure led to a surface with augmented roughness, due to the increased percentage of the TiO_2 , as it was verified from the EDX analysis (Figure 5e,h).

3.2. X-ray Diffraction (XRD) Measurements

XRD patterns of the fabricated materials are presented in Figure 6. The characteristic diffraction peaks of PLA appeared at $2\theta = 14.8^\circ$, 16.5° , 19° , and 22° resulting from the crystal planes (010), (200/110), (203), and (210) [29]. No diffraction peaks appeared in any sample, as thermal processing, such as extrusion and printing, usually leads to amorphous materials [30]. The small crystalline peaks that the coated material exhibits are probably due to the heating during the coating procedure, facilitating some cold crystallization.

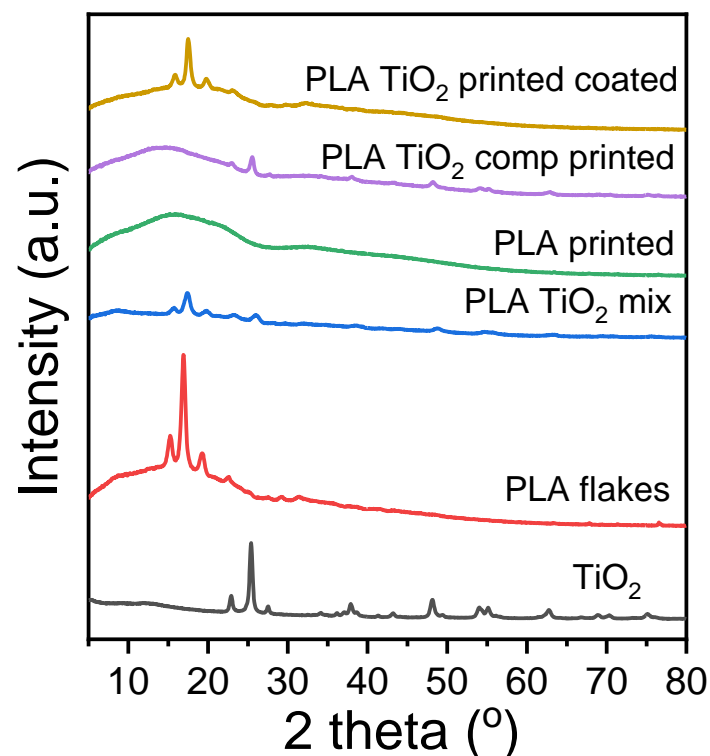


Figure 6. X-ray diffraction patterns of PLA, TiO_2 , and the 3D-printed specimens.

3.3. Differential Scanning Calorimetry (DSC) Measurements

The thermal properties of the fabricated PLA/ TiO_2 materials were determined using DSC analysis. The recorded DSC thermograms upon the first and the second heating scan are presented in Figure 7. The characteristic thermal transitions, including glass transition temperature (T_g), cold crystallization temperature (T_{cc}), and melting point (T_m), as well as the % degree of crystallinity of the materials, are summarized in Table 3. No crystallization peak was observed in any of the samples upon cooling from the melt. As can be observed, all the printed samples exhibited a very low degree of crystallinity, as processing methods, such as printing, tend to erase the matrix crystallinity [30]. All samples were amorphous, showing glass transition at 60 – 62°C , cold crystallization, and subsequent melting. This observation is in agreement with the obtained XRD patterns. Furthermore, a small reduction in the T_g values of the printed samples in comparison to the PLA flakes can be attributed to some degradation during the thermal processing of 3D printing [31]. The

coating process seems to also have an effect on the thermal transitions of the final sample, as T_g and T_m values decreased. However, the thermal transitions of the samples were not significantly affected.

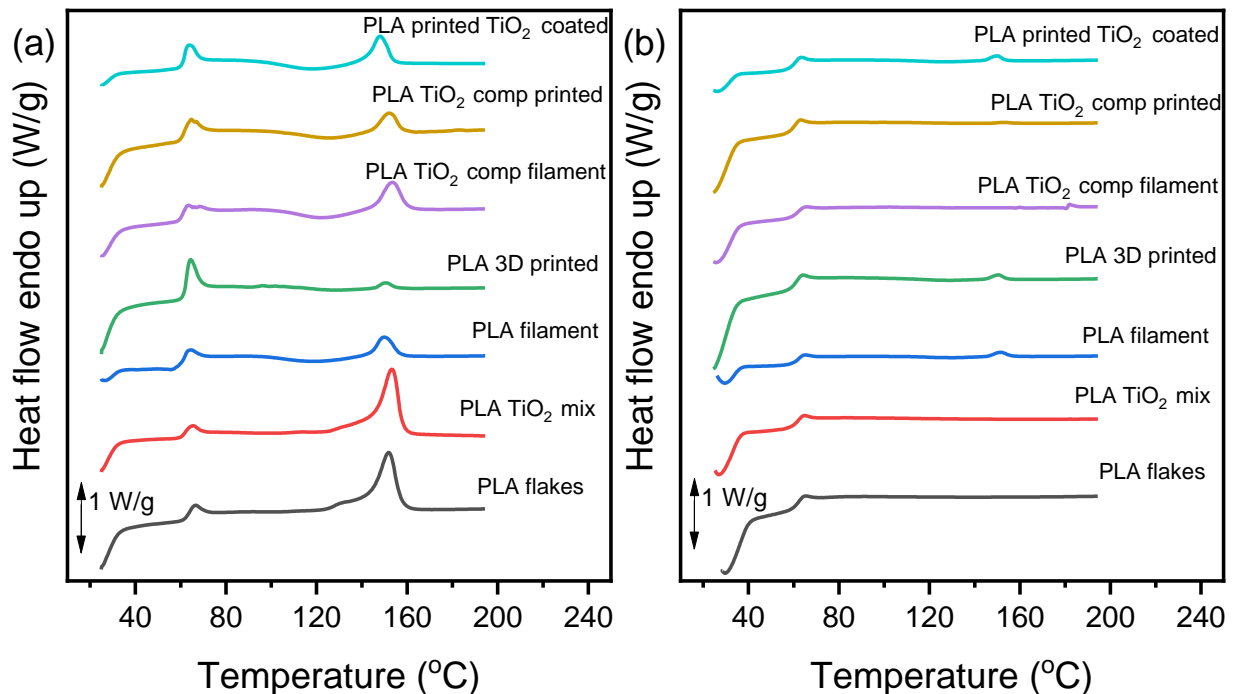


Figure 7. DSC graphs of the materials during heating with rate 20 °C/min, (a) first heating, and (b) second heating scan.

Table 3. Thermal characteristics of the samples as measured by DSC.

Sample	1st Heating				2nd Heating			
	T_g	T_{cc}	T_m	X_c	T_g	T_{cc}	T_m	X_c
PLA flakes	61.9	-	151.9	33.5	60.7	-	-	0
PLA TiO ₂ mix	60.7	-	153.4	35.7	60.5	-	-	0
PLA filament	60.3	118.5	149.8	1.4	63.3	129.1	151.1	0
PLA 3D printed	61	127	150.7	0.0	59.7	127.7	150.7	0
PLA TiO ₂ comp filament	59.9	121.7	153.3	3.0	60.5	-	-	0
PLA TiO ₂ comp printed	61.8	124.7	152	1.1	58.9	-	152.7	0.1
PLA TiO ₂ coated printed	60.1	116.8	148.1	0.5	58.9	125.8	143.1	0

3.4. Contact Angle Measurements

The contact angle of the surface with water plays a key role in the characterization of a material, as it can offer an insight into its absorption and its adhesion profile [32]. The water contact angle of polymeric materials is a function of their chemical composition and surface properties (roughness, heterogeneity, and preparation method), as well as temperature [33]. The hydrophilicity of the PLA/Joncryl (PLA), PLA/Joncryl/TiO₂ (PLA TiO₂ comp), and PLA/Joncryl coated (PLA TiO₂ coated) printed specimens was assessed through water contact angle measurements, and the methodology is illustrated in Figure 8. As can be observed, PLA/Joncryl specimens had a contact angle of ~54.2°. Neat PLA appeared less hydrophobic than expected because of its surface roughness. The addition of TiO₂ to PLA caused a statistically significant decrease in the contact angle values of both the composite and the coated specimen, and a decreasing trend in the values of the

composite to the coated sample. This trend is a result of the increased free energy and the increased roughness of the specimen, as can be assumed from the corresponding SEM images [34]. Furthermore, the hydrophilicity of the incorporated TiO₂ nanoparticles, owing to the unsaturated reactive hydroxyl (-OH) groups, resulted in the significantly enhanced hydrophilicity of the final samples [35,36]. Although the hydrophilic character of a sample is related to its poor resistance to water, this may be beneficial for the contact between the microbial cells and the film which can facilitate the antimicrobial activity.

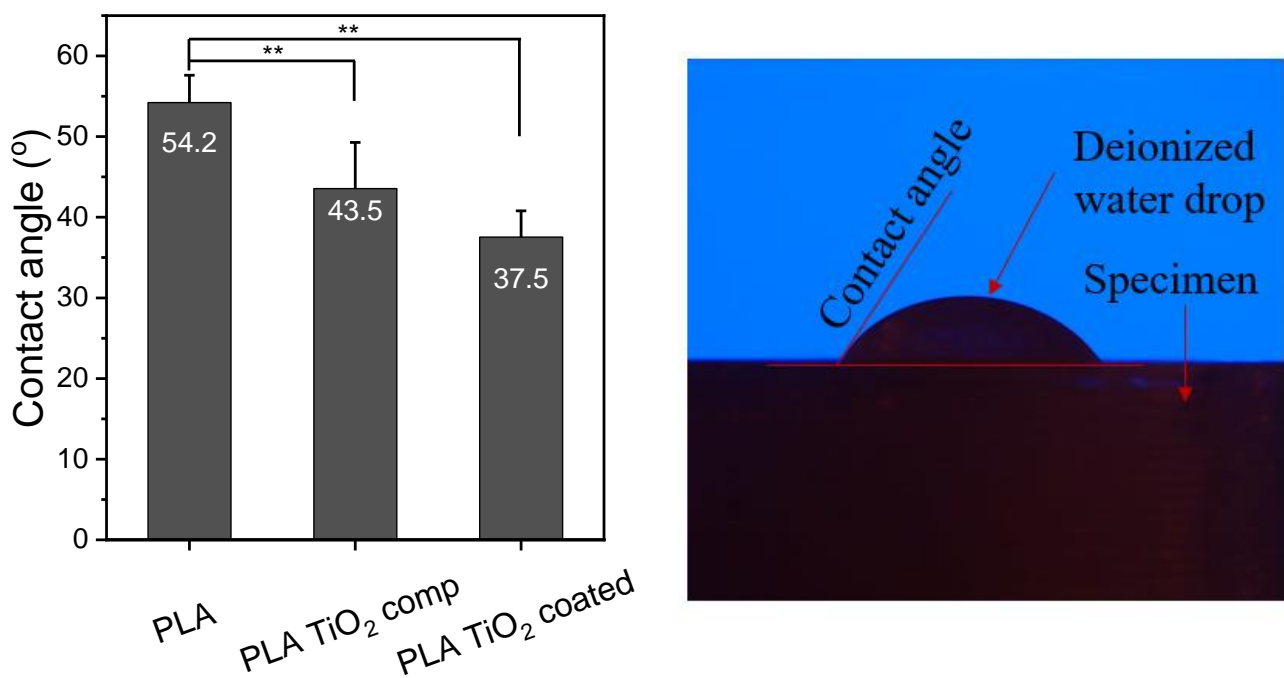


Figure 8. Water contact angle of 3D-printed PLA, PLA TiO₂ comp, and PLA TiO₂ coated. One-way ANOVA, ** p 0.001–0.01.

3.5. Tensile Testing Measurements

As the mechanical features of a polymer define its final applications, tensile tests were performed and the results are presented in Figure 9. In Figure 9a–c, stress–strain diagrams of the three specimen categories demonstrate differences in mechanical properties between specimens printed with PLA/Joncryl (PLA) filament, PLA/Joncryl/TiO₂ (PLA TiO₂ comp) filament, and specimens printed with PLA/Joncryl filament followed by the coating process (PLA TiO₂ coated). The PLA specimens exhibit the highest stress and strain at break, whereas the PLA TiO₂ coated specimens show the highest Young's modulus value. The stress–strain curves indicate that both the integration of TiO₂ nanoparticles and the coating process, aimed at providing antimicrobial properties to the final polymeric material, influence the mechanical properties of the developed filament. This is evident in the stress–strain curves, particularly in the ultimate tensile strength (UTS) or the maximum stress the material can endure before failure. The stress–strain curves of the PLA/Joncryl filament demonstrate the highest ultimate tensile strength. As Figure 9d–f illustrates, there is a statistically significant decrease in tensile strength and strain values among the PLA and either composite. The decreased values of the composite sample can be a result of defects on the printed structure (as shown in Figure 5c). The lower values of tensile strength and strain that the coated sample exhibits, in combination with its increased Young's modulus value, can be attributed to it being soaked in aqueous solution and ammonia, which could have caused some hydrolytic degradation to the material. However, the variation of the Young's modulus values between all samples was insignificant ($p > 0.05$).

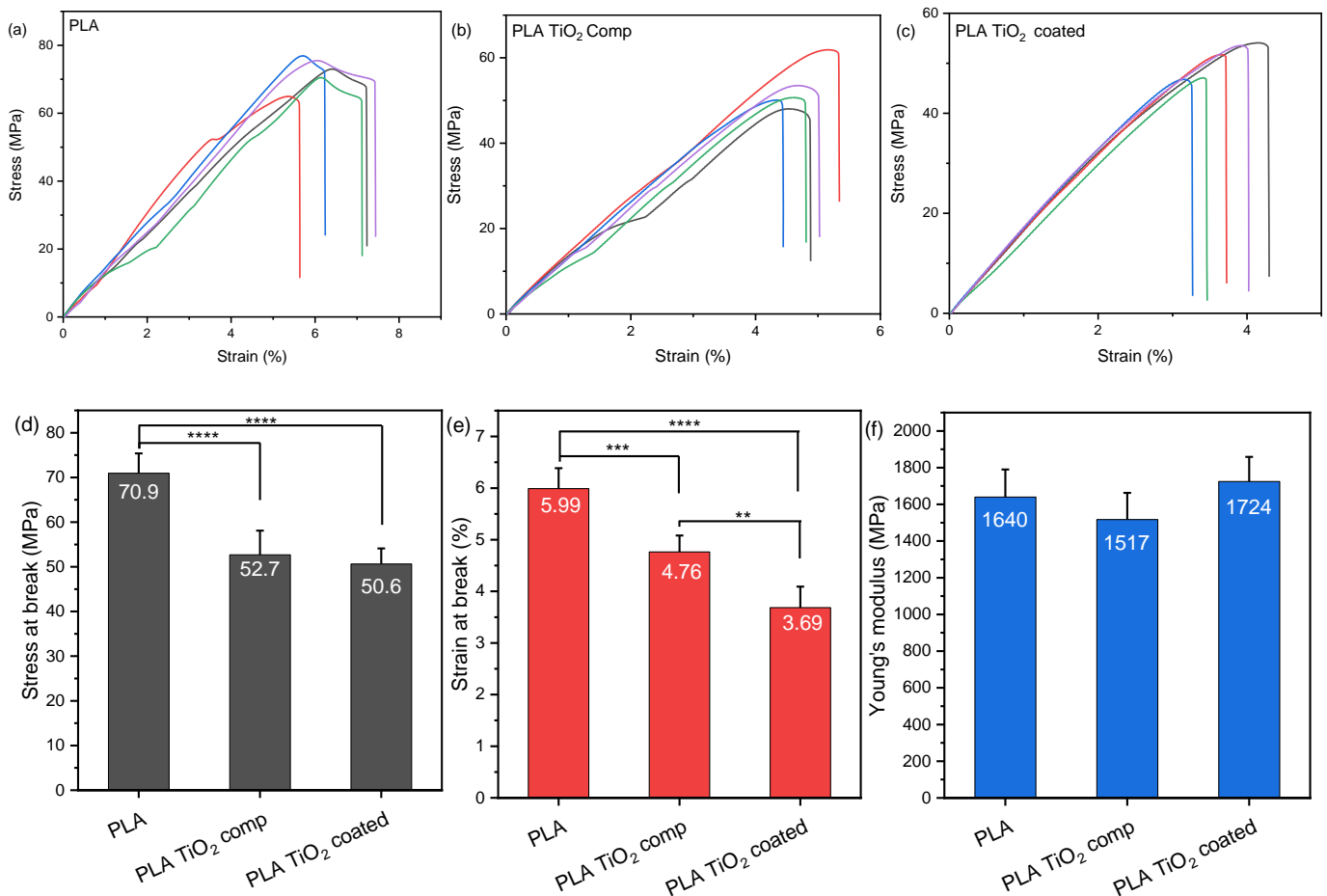


Figure 9. Stress–strain curves of (a) PLA and (b) PLA TiO₂ comp printed specimens, (c) stress at break, (d) strain at break, and (e) Young's modulus values. One-way ANOVA. ** 0.001 < p < 0.01, *** 0.0001 < p < 0.001, **** p < 0.0001.

Generally, the percentage and diameter of the particles incorporated in the matrix strongly affect its final features. It has been reported that the weight fractions of TiO₂ nanoparticles up to 1% increased the tensile strength and strain values, while at high TiO₂ concentrations, the self-networking of nanoparticles can take place [31]. This phenomenon may lead to the agglomeration and non-homogeneous dispersion of the particles [34]. This could potentially indicate that the agglomeration of TiO₂ nanoparticles at high loadings may contribute to the weakening of the mechanical properties, as evidenced in the stress–strain diagram, but it is necessary to achieve antimicrobial properties. Agglomerated nanoparticles restrict the interfacial area between themselves and the polymer matrix, resulting in a non-uniform particle distribution and a reduction in the nanoparticle concentration within the composite. Furthermore, it is found that the functionalization of TiO₂ or the addition of a plasticizer is essential for the improvement of the mechanical features of PLA/TiO₂ materials compared to the neat PLA [37–39]. Similar behavior has been observed with the presence of other metal-based nanoparticles, where concentrations above 1% wt. showed decreased mechanical properties [40–43].

All things considered, the diagrams in Figure 9 reveal that the stress at break (MPa) exhibits a decrease of 25.67% in the specimens printed with the PLA/Joncryl/TiO₂ filament compared to those printed with the PLA/Joncryl filament. Moreover, an additional decrease of 3.98% is observed in specimens printed with the PLA/Joncryl filament and subsequently subjected to a dispersion immersion coating process. A similar reduction is noticed in the strain at break (%) with a decrease of 20.53% when comparing the PLA/Joncryl to PLA/Joncryl/TiO₂ filament and an additional 22.47% decrease after the coating process.

3.6. Antibacterial Testing Measurements

In Figure 10, the x-axis represents the three time points when the cfu/mL was counted (i.e., 0 h, 1 h, and 2 h), while the y-axis represents the % average viability for each bacterium incubated with the different specimens.

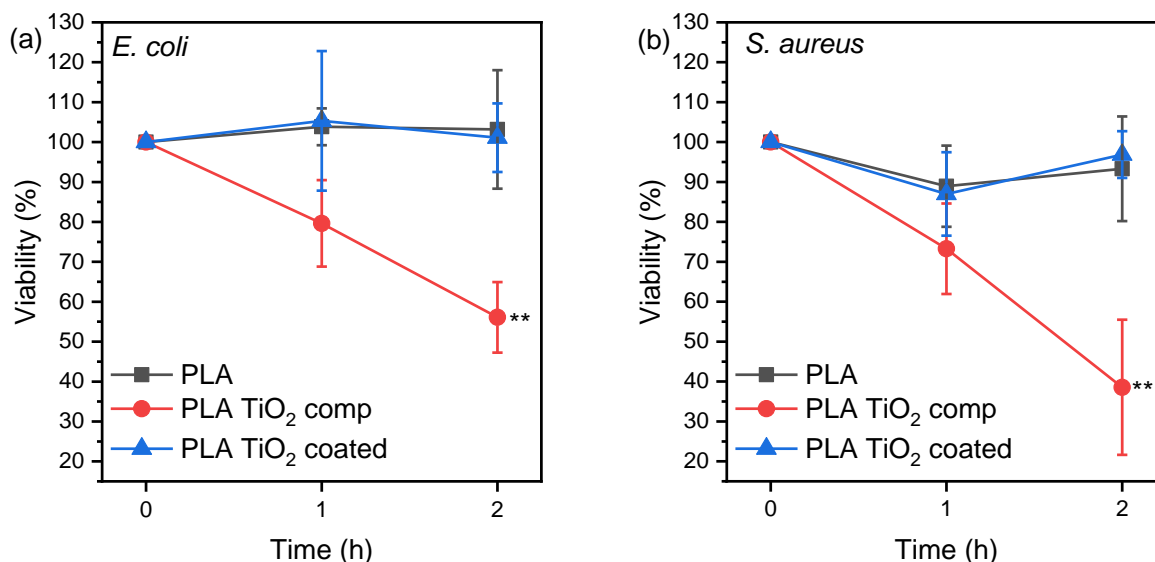


Figure 10. % Viability of bacteria (a) *E. coli* and (b) *S. aureus* after incubation with PLA, PLA TiO₂ comp, and PLA TiO₂ coated specimens. Two-way ANOVA with repeated measurements, ** 0.001 < *p* < 0.01.

The average % viability is calculated as follows: First, the percentage of viability for each replicate is determined by dividing the cfu/mL of each hour by the cfu/mL at hour 0 and then multiplying by 100. Consequently, for each hour, three percentages of viability were obtained (one for each replicate), which were used to calculate the average % viability. These values were used to create the graph.

The results in Figure 10 indicate that the incubation of both bacteria species with the PLA TiO₂ comp specimen caused a statistically significant reduction over time in the microbes' viability compared to PLA and PLA TiO₂ coated specimens. There was no effect on the bacteria strain observed. TiO₂ is hydrophilic, and thus it decreased the water contact angle of PLA TiO₂ comp, but it is also antimicrobial, indicated by its generation of reactive oxygen species when it is exposed to light, which oxidize the cytoplasm of bacteria.

TiO₂ coatings imparted antimicrobial activity when dip-coated on PMMA [44], and their lack of efficiency herein could be due to the leaching of TiO₂ particles from the PLA TiO₂ coated specimen, resulting in a low ion concentration in the incubation medium. Concentration is the most important parameter that affects bacteria survival rate on plastic/metal oxide nanoparticles and the 5 wt.% of TiO₂ added in the PLA TiO₂ filament was effective [45]. Thus, directly adding metal oxides such as TiO₂ is an easy and efficient way of additive manufacturing antimicrobial objects.

4. Conclusions

In this study, we developed two different filaments for FFF feedstock material. One filament is developed for immediate use in 3D printing antibacterial parts, while the other is intended for 3D printing parts and subsequently providing them with antibacterial properties through a coating process. To ensure perfect repeatability in our experiments and the fabrication of all specimens under exactly the same parameters, the stability of all 3D printing parameters was maintained. Deviating from these parameters would lead to different results. To assess the mechanical performance and antibacterial activity of parts manufactured using these two methods, we conducted a series of tests to draw conclusions regarding their structure and properties. Although SEM and optical microscopy images

confirmed the presence of TiO₂ nanoparticles, antibacterial tests demonstrated that only the parts manufactured by PLA/Joncryl/TiO₂ filament exhibited significant antibacterial properties. Interestingly, the coated parts exhibited non-antibacterial activity similar to those printed with the control PLA/Joncryl filament, while the PLA/Joncryl/TiO₂ filament specimens displayed notable antibacterial activity. Consequently, the coating methodology is not recommended, as it does not yield the desired results and involves a more complex procedure requiring access to chemical laboratories, substances, and equipment. In terms of the mechanical attributes of the printed components, the findings indicate that introducing TiO₂ nanoparticles undermines the mechanical properties, leading to the formation of agglomerates. Future studies should investigate the optimal pretreatment method for the materials and the ideal quantity (wt.%) and size of nanoparticles to achieve the best particle distribution and enhance mechanical properties while maintaining antibacterial characteristics.

Given access to the necessary equipment for filament development, this study proposes a DIY method for creating customized antibacterial parts suitable for production on any commercial FFF 3D printer. These parts could include plastic surfaces for various applications in hospitals, medical tools, laboratory plastic parts like Petri dishes, plastic centrifuge test tubes, and pipette tips for cases where reusable antibacterial plastics are applicable. They can also be used in research DIY devices such as bioreactors, orbital shakers, or other costly components that can be replaced with this cost-effective 3D printing solution. Finally, with further research and possible improvements, this proposed filament could be assessed for 3D printing implants or scaffolds to be used in bone reconstruction applications, potentially replacing existing materials used in these applications.

Author Contributions: Conceptualization, S.P. and Z.T.; methodology, E.M.P., D.N.B. and C.K.; software, S.P. and D.T.; validation, S.P., Z.T. and C.K.; formal analysis, S.P., E.X. and G.K.; investigation, S.P., Z.T., G.K. and E.X.; resources, D.N.B., D.T. and C.K.; data curation, S.P., G.K. and E.X.; writing—original draft preparation, S.P. and E.X.; writing—review and editing, Z.T. and E.M.P.; visualization, Z.T.; supervision, E.M.P.; project administration, E.M.P. and D.N.B.; funding acquisition, E.M.P. All authors have read and agreed to the published version of the manuscript.

Funding: Horizon 2020 PestNu project under the GA no. 101037128.

Institutional Review Board Statement: Not applicable.

Informed Consent Statement: Not applicable.

Data Availability Statement: All the data are included in the manuscript.

Acknowledgments: This work supported by the EU Green Deal project PestNu which has received funding from the European Union's Horizon 2020 research and innovation programme under Grant Agreement no. 101037128. The authors would like to thank candidates Chrysanthi Papoulia and Eleni Pavlidou for the SEM observations, as well as Michiel Noordam for the help with the statistical analysis. They would also like to thank Maria Eirini Grigora from I4byDesign Competence Center for her support with the 3devo Composer Series 350/450 filament maker operation.

Conflicts of Interest: The authors declare no conflict of interest.

References

1. Mastura, M.T.; Alkahari, M.R.; Syahibudil Ikhwan, A.K. Life Cycle Analysis of Fused Filament Fabrication: A Review. In *Design for Sustainability*; Elsevier: Amsterdam, The Netherlands, 2021; pp. 415–434. [[CrossRef](#)]
2. Gao, X.; Qi, S.; Kuang, X.; Su, Y.; Li, J.; Wang, D. Fused Filament Fabrication of Polymer Materials: A Review of Interlayer Bond. *Addit. Manuf.* **2021**, *37*, 101658. [[CrossRef](#)]
3. Pechlivani, E.M.; Pemas, S.; Kanlis, A.; Pechlivani, P.; Petrakis, S.; Papadimitriou, A.; Tzovaras, D.; Hatzistergos, K.E. Enhanced Growth of Bacterial Cells in a Smart 3D Printed Bioreactor. *Micromachines* **2023**, *14*, 1829. [[CrossRef](#)]
4. García Plaza, E.; Núñez López, P.; Caminero Torija, M.; Chacón Muñoz, J. Analysis of PLA Geometric Properties Processed by FFF Additive Manufacturing: Effects of Process Parameters and Plate-Extruder Precision Motion. *Polymers* **2019**, *11*, 1581. [[CrossRef](#)]
5. Moreno Nieto, D.; Alonso-García, M.; Pardo-Vicente, M.-A.; Rodríguez-Parada, L. Product Design by Additive Manufacturing for Water Environments: Study of Degradation and Absorption Behavior of PLA and PETG. *Polymers* **2021**, *13*, 1036. [[CrossRef](#)] [[PubMed](#)]

6. Pechlivani, E.M.; Papadimitriou, A.; Pemas, S.; Ntinias, G.; Tzouvaras, D. IoT-Based Agro-Toolbox for Soil Analysis and Environmental Monitoring. *Micromachines* **2023**, *14*, 1698. [[CrossRef](#)]
7. Vidakis, N.; Petousis, M.; Velidakis, E.; Tzounis, L.; Mountakis, N.; Kechagias, J.; Grammatikos, S. Optimization of the Filler Concentration on Fused Filament Fabrication 3D Printed Polypropylene with Titanium Dioxide Nanocomposites. *Materials* **2021**, *14*, 3076. [[CrossRef](#)]
8. Ngo, T.D.; Kashani, A.; Imbalzano, G.; Nguyen, K.T.Q.; Hui, D. Additive Manufacturing (3D Printing): A Review of Materials, Methods, Applications and Challenges. *Compos. Part B Eng.* **2018**, *143*, 172–196. [[CrossRef](#)]
9. Ujfalusi, Z.; Pentek, A.; Told, R.; Schiffer, A.; Nyitrai, M.; Maroti, P. Detailed Thermal Characterization of Acrylonitrile Butadiene Styrene and Polylactic Acid Based Carbon Composites Used in Additive Manufacturing. *Polymers* **2020**, *12*, 2960. [[CrossRef](#)] [[PubMed](#)]
10. Ranakoti, L.; Gangil, B.; Bhandari, P.; Singh, T.; Sharma, S.; Singh, J.; Singh, S. Promising Role of Polylactic Acid as an Ingenious Biomaterial in Scaffolds, Drug Delivery, Tissue Engineering, and Medical Implants: Research Developments, and Prospective Applications. *Molecules* **2023**, *28*, 485. [[CrossRef](#)]
11. Bikiaris, N.D.; Koumentakou, I.; Samiotaki, C.; Meimaroglou, D.; Varytimidou, D.; Karatza, A.; Kalantzis, Z.; Roussou, M.; Bikiaris, R.D.; Papageorgiou, G.Z. Recent Advances in the Investigation of Poly(Lactic Acid) (PLA) Nanocomposites: Incorporation of Various Nanofillers and Their Properties and Applications. *Polymers* **2023**, *15*, 1196. [[CrossRef](#)]
12. Balla, E.; Daniilidis, V.; Karlioti, G.; Kalamas, T.; Stefanidou, M.; Bikiaris, N.D.; Vlachopoulos, A.; Koumentakou, I.; Bikiaris, D.N. Poly(Lactic Acid): A Versatile Biobased Polymer for the Future with Multifunctional Properties—From Monomer Synthesis, Polymerization Techniques and Molecular Weight Increase to PLA Applications. *Polymers* **2021**, *13*, 1822. [[CrossRef](#)] [[PubMed](#)]
13. Elsaka, S.E.; Hamouda, I.M.; Swain, M.V. Titanium Dioxide Nanoparticles Addition to a Conventional Glass-Ionomer Restorative: Influence on Physical and Antibacterial Properties. *J. Dent.* **2011**, *39*, 589–598. [[CrossRef](#)] [[PubMed](#)]
14. Vidakis, N.; Petousis, M.; Mountakis, N.; Maravelakis, E.; Zaoutsos, S.; Kechagias, J.D. Mechanical Response Assessment of Antibacterial PA12/TiO₂ 3D Printed Parts: Parameters Optimization through Artificial Neural Networks Modeling. *Int. J. Adv. Manuf. Technol.* **2022**, *121*, 785–803. [[CrossRef](#)]
15. Tekin, D.; Birhan, D.; Kiziltas, H. Thermal, Photocatalytic, and Antibacterial Properties of Calcinated Nano-TiO₂/Polymer Composites. *Mater. Chem. Phys.* **2020**, *251*, 123067. [[CrossRef](#)]
16. González, E.A.S.; Olmos, D.; Lorente, M.Á.; Vélaz, I.; González-Benito, J. Preparation and Characterization of Polymer Composite Materials Based on PLA/TiO₂ for Antibacterial Packaging. *Polymers* **2018**, *10*, 1365. [[CrossRef](#)]
17. Chen, W.; Nichols, L.; Brinkley, F.; Bohna, K.; Tian, W.; Priddy, M.W.; Priddy, L.B. Alkali Treatment Facilitates Functional Nano-Hydroxyapatite Coating of 3D Printed Polylactic Acid Scaffolds. *Mater. Sci. Eng. C* **2021**, *120*, 111686. [[CrossRef](#)]
18. Pechlivani, E.M.; Papadimitriou, A.; Pemas, S.; Giakoumoglou, N.; Tzouvaras, D. Low-Cost Hyperspectral Imaging Device for Portable Remote Sensing. *Instruments* **2023**, *7*, 32. [[CrossRef](#)]
19. Reinhardt, M.; Kaufmann, J.; Kausch, M.; Kroll, L. PLA-Viscose-Composites with Continuous Fibre Reinforcement for Structural Applications. *Procedia Mater. Sci.* **2013**, *2*, 137–143. [[CrossRef](#)]
20. Trivedi, A.K.; Gupta, M.K.; Singh, H. PLA Based Biocomposites for Sustainable Products: A Review. *Adv. Ind. Eng. Polym. Res.* **2023**, *6*, 382–395. [[CrossRef](#)]
21. Grigora, M.-E.; Terzopoulou, Z.; Tsongas, K.; Bikiaris, D.N.; Tzetzis, D. Physicochemical Characterization and Finite Element Analysis-Assisted Mechanical Behavior of Polylactic Acid-Montmorillonite 3D Printed Nanocomposites. *Nanomaterials* **2022**, *12*, 2641. [[CrossRef](#)]
22. Kahraman, Y.; Alkan Goksu, Y.; Özdemir, B.; Eker Gümüş, B.; Nofar, M. Composition Design of PLA/TPU Emulsion Blends Compatibilized with Multifunctional Epoxy-based Chain Extender to Tackle High Impact Resistant Ductile Structures. *J. Appl. Polym. Sci.* **2022**, *139*, 51833. [[CrossRef](#)]
23. Standau, T.; Nofar, M.; Dörr, D.; Ruckdäschel, H.; Altstädt, V. A Review on Multifunctional Epoxy-Based Joncryl[®] ADR Chain Extended Thermoplastics. *Polym. Rev.* **2022**, *62*, 296–350. [[CrossRef](#)]
24. Grigora, M.-E.; Terzopoulou, Z.; Tsongas, K.; Klonos, P.; Kalafatakis, N.; Bikiaris, D.N.; Kyritsis, A.; Tzetzis, D. Influence of Reactive Chain Extension on the Properties of 3D Printed Poly(Lactic Acid) Constructs. *Polymers* **2021**, *13*, 1381. [[CrossRef](#)]
25. *ASTM D638-14*; Standard Test Method for Tensile Properties of Plastics. ASTM International: West Conshohocken, PA, USA, 2014.
26. Lopera, A.A.; Bezzon, V.D.N.; Ospina, V.; Higuaita-Castro, J.L.; Ramirez, F.J.; Ferraz, H.G.; Orlando, M.T.A.; Paucar, C.G.; Robledo, S.M.; Garcia, C.P. Obtaining a Fused PLA-Calcium Phosphate-Tobramycin-Based Filament for 3D Printing with Potential Antimicrobial Application. *J. Korean Ceram. Soc.* **2023**, *60*, 169–182. [[CrossRef](#)]
27. Nájera, S.E.; Michel, M.; Kim, N.-S. 3D Printed PLA/PCL/TiO₂ Composite for Bone Replacement and Grafting. *MRS Adv.* **2018**, *3*, 2373–2378. [[CrossRef](#)]
28. Nájera, S.; Michel, M.; Kyung-Hwan, J.; Kim, J.N. Characterization of 3D Printed PLA/PCL/TiO₂ Composites for Cancellous Bone. *J. Mater. Sci. Eng.* **2018**, *7*, 417. [[CrossRef](#)]
29. Farid, T.; Herrera, V.N.; Kristiina, O. Investigation of Crystalline Structure of Plasticized Poly (Lactic Acid)/Banana Nanofibers Composites. *IOP Conf. Ser. Mater. Sci. Eng.* **2018**, *369*, 012031. [[CrossRef](#)]
30. Sangiorgi, A.; Gonzalez, Z.; Ferrandez-Montero, A.; Yus, J.; Sanchez-Herencia, A.J.; Galassi, C.; Sanson, A.; Ferrari, B. 3D Printing of Photocatalytic Filters Using a Biopolymer to Immobilize TiO₂ Nanoparticles. *J. Electrochem. Soc.* **2019**, *166*, H3239–H3248. [[CrossRef](#)]

31. Marra, A.; Silvestre, C.; Kujundziski, A.P.; Chamovska, D.; Duraccio, D. Preparation and Characterization of Nanocomposites Based on PLA and TiO₂ Nanoparticles Functionalized with Fluorocarbons. *Polym. Bull.* **2017**, *74*, 3027–3041. [[CrossRef](#)]
32. Hebbar, R.S.; Isloor, A.M.; Ismail, A.F. Contact Angle Measurements. In *Membrane Characterization*; Elsevier: Amsterdam, The Netherlands, 2017; pp. 219–255. [[CrossRef](#)]
33. Yekta-Fard, M.; Ponter, A.B. Factors Affecting the Wettability of Polymer Surfaces. *J. Adhes. Sci. Technol.* **1992**, *6*, 253–277. [[CrossRef](#)]
34. Feng, S.; Zhang, F.; Ahmed, S.; Liu, Y. Physico-Mechanical and Antibacterial Properties of PLA/TiO₂ Composite Materials Synthesized via Electrospinning and Solution Casting Processes. *Coatings* **2019**, *9*, 525. [[CrossRef](#)]
35. Nakamura, R.; Imanishi, A.; Murakoshi, K.; Nakato, Y. In Situ FTIR Studies of Primary Intermediates of Photocatalytic Reactions on Nanocrystalline TiO₂ Films in Contact with Aqueous Solutions. *J. Am. Chem. Soc.* **2003**, *125*, 7443–7450. [[CrossRef](#)]
36. Zhang, X.; Xiao, G.; Wang, Y.; Zhao, Y.; Su, H.; Tan, T. Preparation of Chitosan-TiO₂ Composite Film with Efficient Antimicrobial Activities under Visible Light for Food Packaging Applications. *Carbohydr. Polym.* **2017**, *169*, 101–107. [[CrossRef](#)] [[PubMed](#)]
37. Baek, N.; Kim, Y.T.; Marcy, J.E.; Duncan, S.E.; O’Keefe, S.F. Physical Properties of Nanocomposite Poly(lactic acid) Films Prepared with Oleic Acid Modified Titanium Dioxide. *Food Packag. Shelf. Life* **2018**, *17*, 30–38. [[CrossRef](#)]
38. Foruzanmehr, M.; Vuillaume, P.Y.; Elkoun, S.; Robert, M. Physical and Mechanical Properties of PLA Composites Reinforced by TiO₂ Grafted Flax Fibers. *Mater. Des.* **2016**, *106*, 295–304. [[CrossRef](#)]
39. Zhang, Q.; Li, D.; Zhang, H.; Su, G.; Li, G. Preparation and Properties of Poly(Lactic Acid)/Sesbania Gum/Nano-TiO₂ Composites. *Polym. Bull.* **2018**, *75*, 623–635. [[CrossRef](#)]
40. Zuo, M.; Pan, N.; Liu, Q.; Ren, X.; Liu, Y.; Huang, T.-S. Three-Dimensionally Printed Poly(lactic acid)/Cellulose Acetate Scaffolds with Antimicrobial Effect. *RSC Adv.* **2020**, *10*, 2952–2958. [[CrossRef](#)]
41. Wang, Y.; Wang, S.; Zhang, Y.; Mi, J.; Ding, X. Synthesis of Dimethyl Octyl Aminoethyl Ammonium Bromide and Preparation of Antibacterial ABS Composites for Fused Deposition Modeling. *Polymers* **2020**, *12*, 2229. [[CrossRef](#)]
42. Tylingo, R.; Kempa, P.; Banach-Kopeć, A.; Mania, S. A Novel Method of Creating Thermoplastic Chitosan Blends to Produce Cell Scaffolds by FDM Additive Manufacturing. *Carbohydr. Polym.* **2022**, *280*, 119028. [[CrossRef](#)]
43. Pušnik Črešnar, K.; Aulova, A.; Bikiaris, D.N.; Lambropoulou, D.; Kuzmič, K.; Fras Zemljič, L. Incorporation of Metal-Based Nanoadditives into the PLA Matrix: Effect of Surface Properties on Antibacterial Activity and Mechanical Performance of PLA Nanoadditive Films. *Molecules* **2021**, *26*, 4161. [[CrossRef](#)]
44. Su, W.; Wang, S.; Wang, X.; Fu, X.; Weng, J. Plasma Pre-Treatment and TiO₂ Coating of PMMA for the Improvement of Antibacterial Properties. *Surf. Coat. Technol.* **2010**, *205*, 465–469. [[CrossRef](#)]
45. Abdullah, T.; Qurban, R.O.; Bolarinwa, S.O.; Mirza, A.A.; Pasovic, M.; Memic, A. 3D Printing of Metal/Metal Oxide Incorporated Thermoplastic Nanocomposites With Antimicrobial Properties. *Front. Bioeng. Biotechnol.* **2020**, *8*, 568186. [[CrossRef](#)] [[PubMed](#)]

Disclaimer/Publisher’s Note: The statements, opinions and data contained in all publications are solely those of the individual author(s) and contributor(s) and not of MDPI and/or the editor(s). MDPI and/or the editor(s) disclaim responsibility for any injury to people or property resulting from any ideas, methods, instructions or products referred to in the content.